Surface tension, adsorption and surface entropy of liquid-vapour systems by atomistic simulation

1991 J. Phys.: Condens. Matter 3 3645

(http://iopscience.iop.org/0953-8984/3/20/025)

J. Phys.: Condens. Matter 3 (1991) 3645–3661. Printed in the UK

Surface tension, adsorption and surface entropy of liquid–vapour systems by atomistic simulation

E Salomons and M Mareschal†
CEREM-DTM-SRMP, CEN Saclay, 91191 Gif sur Yvette Cédex, France

Received 3 January 1991, in final form 8 February 1991

Abstract. Results of Monte Carlo and molecular-dynamics simulations of Lennard-Jones systems are presented in order to compare various methods of computing interfacial properties of liquid–vapour systems. For the computation of the surface tension γ a new method is developed, which makes use of the Bennett procedure for calculating free-energy differences. The method is compared with the conventional route to the surface tension via the virial expression. For the temperature derivative of the surface tension, $d\gamma/dT$, both a fluctuation equation and the Gibbs adsorption equation are employed. It is found that $d\gamma/dT$ is determined considerably more accurately by the adsorption equation (through the surface entropy). Results of simulations of binary Lennard-Jones mixtures are also presented. For the argon–krypton system, values of the adsorption of argon at the interface are determined from density profiles, and are compared with values predicted by the adsorption equation. Positive adsorption of argon manifests itself in krypton-rich mixtures as a significant 'bump' in the argon density profile near the interface.

1. Introduction

The microscopic understanding of liquid–vapour systems has increased greatly by the use of computer simulation methods for the computation of thermodynamic interfacial quantities [1]. From simulations of systems with 10^2–10^4 atoms it has been found that the interface has a thickness of typically 2–3 atomic diameters (at temperatures well below the critical temperature). Such microscopic information is not provided by the thermodynamic theory of macroscopic, two-phase systems. Thermodynamics merely provides relations between ensemble averages, which are computed in simulations. In this paper we investigate whether these relations are obeyed by the small liquid–vapour systems used in simulations. Attempts in this direction have already been reported by other authors [2, 3]. However, the present study is more systematic and complete. The systems often consist of a thin liquid film in equilibrium with its vapour, so that finite-size effects are expected to be of particular importance. Further, we investigate whether these relations can be used to compute thermodynamic quantities by alternative, more efficient methods than the methods commonly used.

† Also: Université Libre de Bruxelles, Belgium.

0953-8984/91/203645 + 17 $03.50

The first relation we consider is in fact the definition of the surface tension γ of a liquid–vapour system with a planar interface of area A:

$$\gamma = (\partial F/\partial A)_{N,V,T} \tag{1.1}$$

where F is the free energy of the system. For a system consisting of atoms interacting through a pairwise additive interatomic potential $\varphi(r)$, one can derive from equation (1.1) (see section 2)

$$\gamma = \frac{1}{2A}\left\langle \sum_{i<j}\left(1 - \frac{3z_{ij}^2}{r_{ij}^2}\right) r_{ij}\varphi'(r_{ij})\right\rangle \tag{1.2}$$

where r_{ij} is the distance between atoms i and j, $\varphi'(r_{ij})$ is the derivative of the pair potential, and angular brackets denote an ensemble average. This expression also follows from the definition of the surface tension as the tangential pressure deficit at the interface, by using the virial theorem for the components of the pressure tensor. Equation (1.2) will be referred to as the virial expression of the surface tension. In most simulation studies the surface tension has been determined by using the virial expression [1]. In section 3 it is demonstrated that the surface tension can also be determined directly from the definition (1.1), by computing the change in free energy corresponding to a small isothermal, volume-conserving deformation of the system that enhances the area of the interface. This shows that the values of γ obtained from simulations through the virial expression are consistent with the thermodynamic definition (1.1), and furthermore provides an alternative method to determine the surface tension from simulations, which is, in principle, applicable also to geometries other than the flat interface.

In section 4 we consider the temperature derivative of the surface tension, $\mathrm{d}\gamma/\mathrm{d}T$ (or better $(\partial\gamma/\partial T)_{N,V,A}$). The temperature derivative of a thermodynamic quantity α, which is the canonical average of a microscopic observable $\hat{\alpha}$ (independent of the kinetic energy of the system), is given by the fluctuation equation [4]

$$\mathrm{d}\alpha/\mathrm{d}T = (1/k_B T^2)\langle(\hat{U} - U)\hat{\alpha}\rangle \tag{1.3}$$

where $\hat{U}$ is the potential energy of the system, which fluctuates around an average value U. This equation, which follows directly from the statistical-mechanical definition of phase-space probability density, is commonly used for the computation of specific heats or magnetic susceptibilities from computer simulations. For the surface tension it turns out that equation (1.3) yields $\mathrm{d}\gamma/\mathrm{d}T$ with rather large statistical uncertainty, primarily due to large fluctuations in the microscopic observable $\hat{\gamma}$.

Section 5 deals with the Gibbs adsorption equation [1]

$$\mathrm{d}\gamma = -\eta^s\,\mathrm{d}T - \sum_i \Gamma_i\,\mathrm{d}\mu_i. \tag{1.4}$$

Here η^s is the surface entropy density, and Γ_i and μ_i are the adsorption and chemical potential, respectively, of component i in the system. Previous attempts [2, 3] to verify the adsorption equation by simulation suffered from large error bars. Here we consider first a single-component system, for which the choice of the equimolar dividing surface [1] yields a vanishing second term $\Gamma\,\mathrm{d}\mu$. Values of η^s are compared with values of $\mathrm{d}\gamma/\mathrm{d}T$, and good agreement is obtained. Next, binary mixtures are considered, with interaction parameters appropriate to the argon–krypton system. Choosing the dividing surface so that $\Gamma_{\mathrm{krypton}} = 0$, we compare values of Γ_{argon} with values of $\mathrm{d}\gamma/\mathrm{d}\mu_{\mathrm{argon}}$ (at constant temperature). Reasonable agreement is obtained.

In the simulations discussed in this paper, the Lennard-Jones interatomic potential has been used:

$$\varphi(r) = \begin{cases} 4\varepsilon[(\sigma/r)^{12} - (\sigma/r)^6] & \text{if } r < R_c \\ 0 & \text{if } r \geq R_c \end{cases} \tag{1.5}$$

where R_c is the cut-off radius. Both the Monte Carlo method and the molecular-dynamics method have been used. In Monte Carlo simulations the truncated, discontinuous potential (1.5) is used. In molecular-dynamics simulations non-singular forces are used (i.e. the delta function at $r = R_c$ is ignored), corresponding to a shifted, continuous potential. Hence, in molecular-dynamics simulations a different interatomic potential is used than in Monte Carlo simulations, and molecular-dynamics results cannot be compared with Monte Carlo results. In some cases (section 3) a long-range correction to the surface tension is applied, to account for the neglected tail of the Lennard-Jones potential. In these cases values of the surface tension are representative of a system with the full interatomic potential. In the other cases (sections 4 and 5) this long-range correction is not applied, so there the results are representative of either a system with a truncated potential (in the case of Monte Carlo simulations) or a system with a truncated and shifted (continuous) potential (in the case of molecular-dynamics simulations).

Dimensionless reduced quantities are used in this paper, and defined as follows (reduced quantities are indicated with an asterisk):

length	$L^* = L/\sigma$
energy	$E^* = E/\varepsilon$
entropy	$S^* = S/k_B$
temperature	$\tau \equiv T^* = k_B T/\varepsilon$
surface tension	$\gamma^* = \gamma\sigma^2/\varepsilon$
density	$\rho^* = N\sigma^3/V$
adsorption	$\Gamma^* = \Gamma\sigma^2$.

(1.6)

The asterisk will be omitted for simplicity.

2. Virial expression of the surface tension

In this section the virial expression of the surface tension [1, 5, 6] is derived by evaluating the change in free energy due to an isothermal, volume-conserving deformation of the system shown in figure 1. Further, we discuss the typical accuracy one obtains in using this expression in computer simulations.

2.1. Derivation of the virial expression

We consider a liquid–vapour system consisting of N atoms of mass m, enclosed in a volume $V = L_x L_y L_z$ with periodic boundary conditions in the x, y and z directions (see figure 1). The derivation given here is restricted to systems with planar liquid–vapour

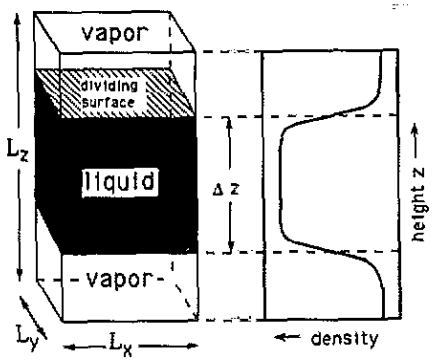

Figure 1. Liquid–vapour system used in simulations described in this paper, with corresponding density profile (schematic).

interfaces (as shown in figure 1) and pairwise additive interatomic potentials $\varphi(r)$. In the absence of an external field, the potential energy of the system reads

$$U(\boldsymbol{r}^N) = \sum_{i<j} \varphi(r_{ij}). \tag{2.1}$$

The free energy of the system, $F(N, V, T, A)$, is given by

$$\exp[-\beta F(N, V, T, A)] = \frac{\Lambda^{3N}}{N!} \int_V \mathrm{d}\boldsymbol{r}^N \exp[-\beta U(\boldsymbol{r}^N)] \tag{2.2}$$

where $\Lambda = (2\pi m k_B T/h^2)^{1/2}$ and $\beta = (k_B T)^{-1}$. We consider the following coordinate transformation $\boldsymbol{r} \rightarrow \boldsymbol{r}'$:

$$x' = x(1+\varepsilon) \qquad y' = y(1+\varepsilon) \qquad z' = z(1+\varepsilon)^{-2} \tag{2.3}$$

which keeps the volume V constant and enhances the interface area $A = 2L_xL_y$ by an amount

$$\Delta A_\varepsilon = A(2\varepsilon + \varepsilon^2). \tag{2.4}$$

From the definition (1.1) of the surface tension γ, it follows that

$$\gamma = \lim_{\varepsilon \to 0} \frac{F(N, V, T, A + \Delta A_\varepsilon) - F(N, V, T, A)}{\Delta A_\varepsilon}. \tag{2.5}$$

Here $F(N, V, T, A + \Delta A_\varepsilon)$ is the free energy of the system after the transformation, which is determined by applying transformation (2.3) to equation (2.2) and expanding in powers of ε:

$$\exp[-\beta F(N, V, T, A + \Delta A_\varepsilon)] = \frac{\Lambda^{3N}}{N!} \int_V \mathrm{d}\boldsymbol{r}'^N \exp[-\beta U(\boldsymbol{r}'^N)]$$

$$= \frac{\Lambda^{3N}}{N!} \int_V \mathrm{d}\boldsymbol{r}^N \exp[-\beta U(\boldsymbol{r}^N)] \left(1 - \beta \sum_{i<j} \varphi'(r_{ij})(r'_{ij} - r_{ij}) + \mathrm{O}((r'_{ij} - r_{ij})^2)\right) \tag{2.6}$$

where

$$r'_{ij} = r_{ij}[1 - \varepsilon(1 - 3z_{ij}^2/r_{ij}^2) + \mathrm{O}(\varepsilon^2)] \tag{2.7}$$

in which the terms $\mathrm{O}((r'_{ij} - r_{ij})^2)$ and $\mathrm{O}(\varepsilon^2)$ contain second- and higher-order terms,

and it has been used that the Jacobian of transformation (2.3) is equal to unity. One obtains from equations (2.2), (2.5), (2.6) and (2.7) the virial expression of the surface tension:

$$\gamma = \frac{1}{2A}\left\langle \sum_{i<j}\left(1 - \frac{3z_{ij}^2}{r_{ij}^2}\right) r_{ij}\varphi'(r_{ij})\right\rangle \tag{2.8}$$

where angular brackets denote an ensemble average.

2.2. *Statistical uncertainty*

Identifying an ensemble average α with the time average $\langle\hat{\alpha}\rangle$ obtained from a simulation run with a length of T time steps, one can estimate the statistical uncertainty in α by the following expression for the standard deviation s:

$$s^2 = (\langle\hat{\alpha}^2\rangle - \alpha^2)/(T/t_c) \tag{2.9}$$

in which t_c is the correlation time. The numerator in this expression is obtained directly from the simulation, and the correlation time can be determined as follows [4]. The run of T time steps is divided into n_b consecutive blocks of length t_b (so that $n_b t_b = T$), and values of $\hat{\alpha}$ in each block are used to compute block averages α_b. One defines the correlation time by

$$t_c = \lim_{t_b\to\infty}\left[t_b s^2(t_b)/s^2(t_b = 1)\right] \tag{2.10}$$

with

$$s^2(t_b) = \frac{1}{n_b}\sum_{b=1}^{n_b}(\alpha_b - \alpha)^2. \tag{2.11}$$

In practice, one determines t_c as the asymptotic value of a plot of $t_b s^2(t_b)/s^2(t_b = 1)$ against $t_b^{1/2}$.

We now consider the statistical uncertainty in the surface tension of the system shown in figure 1, as determined by molecular dynamics (MD) using the virial expression (2.8). For a system of 256 or 500 atoms, at temperature $\tau = 0.9$, a correlation time of $t_c \simeq 30$ MD steps (1 MD step $= 10^{-14}$ s) is found, and $(\langle\hat{\gamma}^2\rangle - \gamma^2) \simeq 1.2$, so that the standard deviation is $s \simeq 5.7/T^{1/2}$, or $s \simeq 0.02$ for a run of $T = 10^5$ MD steps. This estimate appears to be slightly too low to account for the spread in values of γ we obtained from different simulations (by a factor of 2 at most; see e.g. tables 2 and 3 in section 4). The estimate of the correlation time, $t_c \simeq 30$ MD steps, is confirmed by a plot of the time correlation function of the surface tension, $\langle\gamma_0\gamma_t\rangle$, shown in figure 2. One sees that $\langle\gamma_0\gamma_t\rangle$ decays in a time of approximately 30 MD steps.

The above discrepancy (a factor of 2) might originate from the correlation between $\hat{\gamma}$ and $\hat{U}$ implied by equation (1.3). The correlation time for the potential energy U is an order of magnitude larger than for the surface tension γ. This might result in a small but

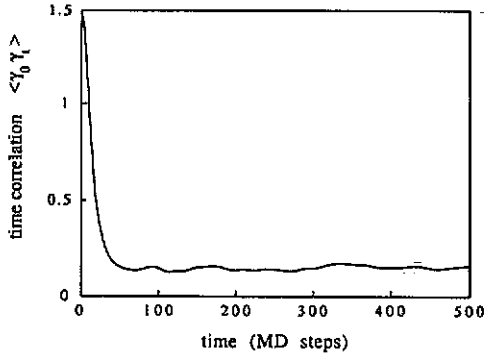

Figure 2. Time correlation function $\langle \gamma_0 \gamma_t \rangle$ as a function of time t, for a system of 500 atoms at temperature $\tau = 0.9$, obtained from a molecular-dynamics run of 2.5×10^5 MD steps.

persistent effect on $\hat{\gamma}$, which is not taken into account in the estimate given by equation (2.9).

3. New method to determine the surface tension

In most simulation studies of the liquid–vapour interface the surface tension γ was determined using the virial expression (2.8). In this section it will be shown that γ can also be determined directly using the definition

$$\gamma = (\partial F/\partial A)_{N,V,T}. \tag{3.1}$$

This direct approach is in the spirit of the method devised by Miyazaki *et al* [7], which makes use of the relation [1]

$$\gamma = F^s/A \tag{3.2}$$

where F^s is the surface free energy of a liquid–vapour interface with area A. The latter method employs a rather complicated scheme to create a free surface in a bulk liquid. The method proposed here is relatively simple.

3.1. Description of the method

For the simulations either the Monte Carlo or the molecular-dynamics technique can be used. The system, shown in figure 1, consists of a liquid film in equilibrium with its vapour, contained in a rectangular box with sides of length L_x, L_y and L_z. The total interface area is equal to $A = 2L_xL_y$. Periodic boundary conditions are used in the x, y and z directions.

In order to compute the surface tension from equation (3.1), we consider again the following isothermal, volume-conserving coordinate transformation:

$$x' = x(1 + \varepsilon) \qquad y' = y(1 + \varepsilon) \qquad z' = z(1 + \varepsilon)^{-2} \tag{3.3}$$

where ε is a parameter ($\varepsilon \ll 1$). This transformation enhances the interface area by an amount $\Delta A = A(2\varepsilon + \varepsilon^2)$. We will determine the free-energy change ΔF corresponding to the transformation. This is not straightforward, as the free energy cannot be expressed as a statistical ensemble average of a microscopic quantity. Bennett [8] has developed a

general method to determine free-energy differences from simulations. Bennett's method makes use of the energy difference

$$\Delta\hat{U} = \hat{U}_1 - \hat{U}_0 \tag{3.4}$$

where $\hat{U}_1$ and $\hat{U}_0$ are the potential energies of two systems that have the same configurational phase space but different Hamiltonians. The method also works for two systems that are related by a geometrical transformation: transformation (3.3) in the present case. Two histograms of the quantity $\Delta\hat{U}$ are recorded in simulations of the system: one using the original box and one using the transformed box. The free-energy difference ΔF is determined afterwards by solving numerically the implicit equation

$$\langle f(-\beta\Delta\hat{U} + \beta\Delta F)\rangle_1 = \langle f(\beta\Delta\hat{U} - \beta\Delta F)\rangle_0 \tag{3.5}$$

in which $\beta = (k_B T)^{-1}$, $f(x) = [1 + \exp(x)]^{-1}$ is the Fermi function, and angular brackets denote an ensemble average (index 0 refers to the original box, index 1 to the deformed box).

The statistical error in the value of ΔF increases with decreasing overlap of the two histograms [8]. In the present case the overlap can be 'tuned' by the parameter ε: for $\varepsilon = 0$ the overlap is complete, while for increasing ε the overlap decreases. This implies that ε should not be chosen too large. On the other hand, the absolute value of ΔF decreases with decreasing ε ($\Delta F = 0$ for $\varepsilon = 0$), so that the relative error in ΔF is expected to increase for ε decreasing to zero. Hence there is an optimum value for ε. By performing simulations using different values of ε the optimum value was found to be in the range $\varepsilon = 0.005$–0.01 (at least for the system considered in the next section).

3.2. Application of the method

We have applied the method described in the previous section to the Lennard-Jones system. Simulations were performed by the Monte Carlo method. A simulation box with sides of length $L_x = 10.8$, $L_y = 10.8$ and $L_z = 21.6$ was used, with 1000 atoms. The liquid film had a thickness of about $\Delta z = 10$. For the potential a cut-off radius of $R_c = 5$ was employed.

The system was allowed to reach equilibrium by performing 0.5×10^4 Monte Carlo steps per atom. The actual simulations had a length of 2×10^4 Monte Carlo steps per atom. The surface tension was determined afterwards by the method described in the previous section. We also determined density profiles $\rho(z)$. Values of the bulk liquid density ρ^{liq} were found to be close to values of ρ_∞^{liq} obtained from simulations of homogeneous systems. (This point is discussed by Rowlinson and Widom [1]; for smaller values of the cut-off radius than the value $R_c = 5$ used here, one finds that ρ^{liq} is smaller than ρ_∞^{liq}: see also section 5.1).

In table 1 the obtained values of the surface tension γ are presented. Values of the long-range correction term γ_{corr}, which represents the contribution of the potential for distances larger than the cut-off radius R_c, are also given in table 1. This term was calculated by the expression [9]

$$\gamma_{corr} = \tfrac{3}{2}\pi(\rho^{liq}/R_c)^2 \tag{3.6}$$

which is based on the approximation that the pair distribution function $g(r) \simeq 1$ for $r > R_c$. The sum $\gamma + \gamma_{corr}$, which represents the surface tension for the full Lennard-Jones potential, is plotted in figure 3 as a function of temperature. For comparison, two results that were determined by the virial expression (2.8) are included in figure 3: one

Table 1. Surface tension γ of the Lennard-Jones system at different temperatures, obtained from Monte Carlo simulations using equation (3.1). The long-range correction term γ_{corr} is also indicated.

τ	γ	γ_{corr}
0.6867	1.081	0.136
0.7	0.982	0.136
0.75	1.016	0.130
0.8	0.821	0.124
0.85	0.746	0.116
0.9	0.611	0.109
0.95	0.454	0.102
1.0	0.450	0.095
1.05	0.330	0.087
1.1	0.237	0.080

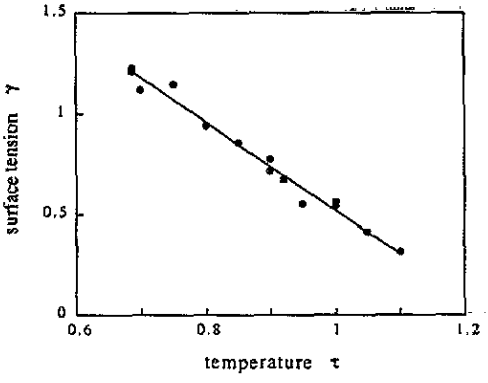

Figure 3. Surface tension γ (including the long-range correction) as a function of temperature τ for the Lennard-Jones system: (●) obtained from Monte Carlo simulations using equation (3.1); (■) obtained from molecular-dynamics simulations using the virial expression (2.8).

obtained from a molecular-dynamics simulation described in section 5.1 (using a system with 864 atoms, a temperature of $\tau = 1.0$ and a cut-off radius of $R_c = 5$), and one reported in the molecular-dynamics study of Nijmeijer *et al* [10] (using $\tau = 0.92$ and $R_c = 7.33$; a long-range correction term of $\gamma_{corr} = 0.05$ has been taken into account). Strictly speaking, molecular-dynamics values cannot be compared with Monte Carlo values, since molecular-dynamics values represent a system with a shifted interatomic potential (see section 1). Nevertheless, the agreement in figure 3 implies that for a cut-off radius of $R_c = 5$ the surface tension is not significantly affected by shifting the potential.

The points in figure 3 shows a statistical scatter of about $\Delta\gamma = \pm 0.05$. This means that the statistical accuracy of the surface tension determined by the method proposed here is comparable to the accuracy obtained by using the virial expression. It should be noted that, although application of the method is simple compared with application of the method of Miyazaki *et al* [7], it is still more complicated than using the virial expression.

4. Temperature derivative of the surface tension

As mentioned in section 1, the temperature derivative of the surface tension is given by

Table 2. Total averages and subaverages for a Lennard-Jones system ($R_c = 3$) of 256 atoms at temperature $\tau = 0.9$, obtained from a molecular-dynamics run of 2.5×10^5 MD steps. No long-range correction has been included in the values.

Interval (10^3 MD steps)	γ	$d\gamma/d\tau$
0–250	0.398	-2.4 ± 0.5
0–62.5	0.395	−2.7
62.5–125	0.419	−3.1
125–187.5	0.362	−1.7
187.5–250	0.415	−1.8

Table 3. Total averages and subaverages for a Lennard-Jones system ($R_c = 3$) of 500 atoms at temperature $\tau = 0.8$, obtained from a molecular-dynamics run of 1.0×10^5 MD steps. No long-range correction has been included in the values.

Interval (10^3 MD steps)	γ	$d\gamma/d\tau$
0–100	0.585	-2.2 ± 1.0
0–25	0.542	−1.2
25–50	0.532	−4.3
50–75	0.661	−4.0
75–100	0.604	−0.3

the fluctuation equation

$$d\gamma/dT = (1/k_B T^2)\langle(\hat{U} - U)\hat{\gamma}\rangle \tag{4.1}$$

where $\hat{\gamma}$ is the microscopic observable defined by the virial expression (2.8) of the surface tension. This equation follows directly by differentiating the virial expression with respect to the temperature. An alternative approach [11] is to make use of the general relation

$$\gamma(T') = \langle\hat{\gamma}\exp[-(\beta' - \beta)\hat{U}]\rangle_T / \langle\exp[-(\beta' - \beta)\hat{U}]\rangle_T \tag{4.2}$$

which allows the surface tension at temperature T' to be determined from a simulation at temperature T (here $\beta = (k_B T)^{-1}$). One recovers equation (4.1) by using relation (4.2) in the definition

$$d\gamma/dT = \lim_{T' \to T} \{[\gamma(T') - \gamma(T)]/(T' - T)\}. \tag{4.3}$$

In the following we will compare values of $d\gamma/d\tau$ (τ is the reduced temperature) computed with the fluctuation equation (4.1) with the value of $d\gamma/d\tau$ obtained from values of γ at different temperatures. Molecular-dynamics simulations were performed on the system shown in figure 1, using a shifted Lennard-Jones potential with cut-off radius $R_c = 3$, and an integration time step of 10^{-14} s. Either the Nosé algorithm [12] or the momentum-scaling algorithm [13] was used to fix the temperature. Values of γ and $d\gamma/d\tau$ for a system of 256 atoms at temperature $\tau = 0.9$ are represented in table 2 and for a system of 500 atoms at temperature $\tau = 0.8$ in table 3. The values of $d\gamma/d\tau$ are in

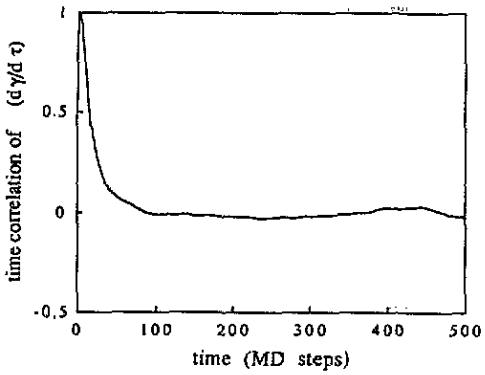

Figure 4. Time correlation function $\langle (d\gamma/d\tau)_0 (d\gamma/d\tau)_t \rangle$ as a function of time t (normalized to the value at $t = 0$), for a system of 500 atoms at temperature $\tau = 0.9$, obtained from a molecular-dynamics run of 10^5 MD steps.

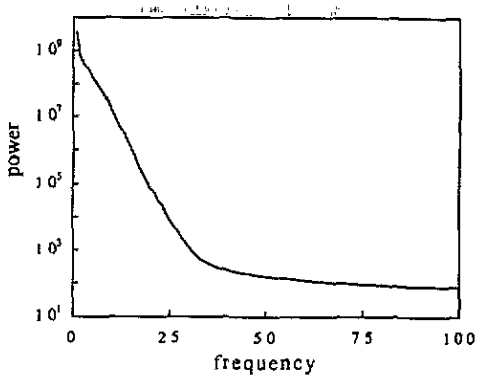

Figure 5. Power spectrum of the microscopic observable $\hat{\theta}$ corresponding to $d\gamma/d\tau$, for a system of 500 atoms at temperature $\tau = 0.9$, obtained from a molecular-dynamics run of 10^5 MD steps. The dimensionless frequency is scaled so that a value of 100 corresponds to a time interval of 2 MD steps.

agreement with the value obtained from values of γ at different temperatures: $d\gamma/d\tau = -1.9 \pm 0.1$ (see section 5.2). However, the statistical error in the value of $d\gamma/d\tau$ computed from equation (4.1) is quite large, as demonstrated by the subaverages in tables 2 and 3. In other words, $d\gamma/d\tau$ is determined more accurately from values of γ at two or three different temperatures than from equation (4.1).

If one assumes that $\hat{\theta} \equiv \delta \hat{U} \hat{\gamma}/\tau^2$, the microscopic observable corresponding to $d\gamma/d\tau$ (see equation (4.1)), obeys Gaussian statistics, then one can use the statistical analysis of section 2.2 to determine the standard deviation in $d\gamma/d\tau$. One obtains typically $(\langle \hat{\theta}^2 \rangle - \theta^2)^{1/2} \simeq 75$, while the correlation time is about $t_c \simeq 50$ MD steps, as demonstrated by the time correlation plot in figure 4. These values yield a standard deviation of $s \simeq 500/T^{1/2}$ (see equation (2.9)), or $s \simeq 2$ for a time interval of 5×10^4 MD steps. This estimate is in fair agreement with the variation in the subaverages in tables 2 and 3.

To get a better understanding of the fluctuations in $d\gamma/d\tau$ we have determined the power spectrum of $\hat{\theta}$, which is shown in figure 5 (the power is defined as the squared modulus of the Fourier transform with respect to time). Clearly most of the power is concentrated in the low-frequency region, and is negligible above a frequency that corresponds to a time interval of about 10 MD steps. Possibly fluctuations of hydrodynamic origin (due to capillary waves) play a role here. Another approach we followed was to replace the instantaneous values of $\hat{\theta}$ in equation (4.1) by subaverages over time intervals of 10, 50 or 100 MD steps. This reduces considerably the amplitude of short-time fluctuations in the accumulated average of the observable $\hat{\theta}$ (defined as $(1/t) \sum_{i=1}^{t} \hat{\theta}_i$). However, it does not affect long-time oscillations in the accumulated average. Consequently, the use of subaverages does not lead to a significant suppression of the large statistical fluctuation in the final average of $\hat{\theta}$.

5. Gibbs adsorption equation

In a liquid–vapour system with M components, changes in the surface tension γ are related to changes in the temperature τ and the chemical potentials μ_i $(i = 1, \ldots, M)$

by the Gibbs adsorption equation [1]

$$d\gamma = -\eta^s \, d\tau - \sum_{i=1}^{M} \Gamma_i \, d\mu_i \tag{5.1}$$

in which η^s is the surface entropy density and Γ_i is the adsorption of component i. In deriving this equation one divides the system into three parts: a bulk liquid part, a bulk vapour part and a surface layer. The small systems used in computer simulations contain a relatively very thick surface layer, in particular at high temperature (the thickness of the surface layer diverges as the temperature approaches the critical temperature). Further, if the system shown in figure 1 is used, one has a liquid film with a thickness of typically only 10 atomic diameters. In such a small system significant deviations from macroscopic equations such as equation (5.1) might occur. This point is investigated in this section. It should be emphasized that we do *not* investigate finite-size effects on the values of thermodynamic quantities (which are probably not negligible for the small systems considered here).

Previously Chapela *et al* [2] and Lee *et al* [3] have attempted to compare results of simulations with predictions of the Gibbs adsorption equation. Large error bars prevented these attempts from being very accurate. The error bars originate predominantly from statistical uncertainties in the bulk liquid and vapour densities, owing to the fact that density profiles obtained from simulations show considerable spatial fluctuations.

In section 5.1 some general points concerning density profiles are discussed. In sections 5.2 and 5.3 results of simulations are presented for pure Lennard-Jones systems and Lennard-Jones mixtures, which are discussed in the light of the Gibbs adsorption equation.

5.1. Density profiles

We consider again a liquid film in equilibrium with its vapour, contained in a rectangular box with periodic boundary conditions in the x, y and z directions (see figure 1). The density profile $\rho(z)$ is determined in a simulation by dividing the system into a number of slabs (e.g. 100) perpendicular to the z axis, and recording a histogram of the number of particles $n(z)$ in each slab. By averaging over a simulation length of typically 10^5 moves per particle (either using the Monte Carlo or the molecular-dynamics method), one obtains a density profile with relatively small spatial fluctuations. The fluctuations in the instantaneous profile are much larger, owing to the small number of particles used in simulations ($N = 10^2$–10^4). For a mixture, the partial density profiles $\rho_i(z)$ ($i = 1, \ldots, M$) are determined in the same way.

It is important that the centre of mass is kept fixed in the simulation. If this is not done spurious effects occur: the surface layer is thickened, the bulk liquid density is lowered and the bulk vapour density is enhanced (This is readily understood from the fact that a uniform density profile would be obtained from a long simulation run if the centre of mass were to move freely throughout the system.)

At first sight, the centre of mass is automatically fixed in a molecular-dynamics simulation by initially setting the total momentum of the system equal to zero. However, this is not true, as a consequence of the periodic boundary conditions: boundary crossings are not exactly balanced. Therefore the centre of mass should be shifted back to its original position after each, say, 10 moves per particle (this amounts to performing the

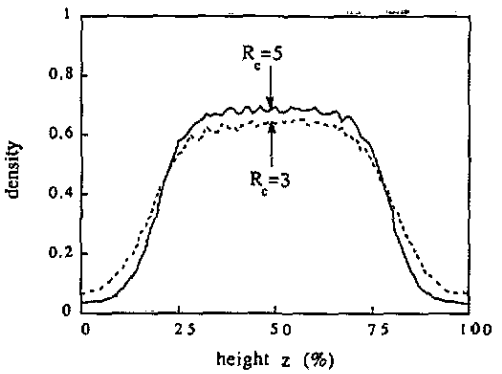

Figure 6. Effect of the cut-off radius R_c on the density profile of the Lennard-Jones system at temperature $\tau = 1.0$, using 864 atoms and a simulation box with $L_x = 10.1$, $L_y = 10.1$ and $L_z = 20.2$. The profiles were determined by molecular-dynamics runs of 2.5×10^4 integration steps.

simulation in the centre-of-mass frame). The same should be done in a Monte Carlo simulation, to eliminate random movements of the centre of mass.

In simulations of mixtures a more serious problem occurs: owing to slow interdiffusion of different components, long runs are required to obtain reproducible, well-averaged partial density profiles. For example, a molecular-dynamics run of 10^5 integration steps is not long enough for the argon–krypton system with 256 atoms at temperature $\tau = 0.9$ (this system is considered in section 5.3), and yields asymmetric partial density profiles. To enhance the interdiffusion we used the following variant of the Monte Carlo method: in addition to conventional displacements of atoms we allow also pairs of dissimilar atoms to exchange positions. Both displacements and exchanges are accepted or rejected according to a transition probability satisfying detailed balance. We found that this method gives a more efficient determination of partial density profiles, as a consequence of a better sampling of configurational phase space.

Finally it is demonstrated how density profiles are affected by the value of the cut-off radius R_c of the potential. For the Lennard-Jones system values ranging from $R_c = 2.5$ to $R_c = 7.33$ have been used by different authors. The density profiles represented in figure 6, for $R_c = 3$ and $R_c = 5$, show that with decreasing R_c the liquid density decreases and the vapour density increases. This effect originates from the fact that a smaller cut-off radius corresponds to neglecting a larger part of the attractive tail of the Lennard-Jones potential, thereby reducing the critical temperature and the region of coexistence in the temperature–density phase diagram. This implies that long-range correction terms for thermodynamic quantities, such as expression (3.6) for the surface tension, account only partially for the effect of the cut-off radius on these quantities. The fact that the density profile is affected by the cut-off radius is not accounted for by these terms.

5.2. Surface entropy

For a pure system the adsorption equation (5.1) reads

$$d\gamma = -\eta^s \, d\tau - \Gamma \, d\mu. \tag{5.2}$$

The surface entropy density η^s and the adsorption Γ depend on the choice of the dividing surface separating the liquid from the vapour [1] (see figure 1). We choose the dividing surface so that the adsorption vanishes: $\Gamma = 0$. Then it follows from equation (5.2) that

$$\eta^s = -(d\gamma/d\tau). \tag{5.3}$$

Table 4. Surface tension γ and surface entropy density η^s of the (truncated and shifted) Lennard-Jones system at different temperatures τ, obtained from molecular-dynamics simulations.

τ	γ	η^s
0.687	0.736	1.984
0.75	0.668	1.843
0.8	0.559	1.878
0.85	0.490	1.672
0.9	0.365	1.642

For this choice of the dividing surface one also has the relation [1] $\gamma = \Psi^s$, where Ψ^s is the surface free-energy density. Hence the surface entropy density can be determined from the relation

$$\eta_s = (\varphi^s - \gamma)/\tau \tag{5.4}$$

in which

$$\varphi^s = (U - u^{liq}V^{liq} - u^{vap}V^{vap})/A \tag{5.5}$$

is the surface potential energy density. Here U is the potential energy of the liquid–vapour system, u^{liq} and u^{vap} are the bulk liquid and vapour potential energy densities (i.e. $u \equiv \delta U/\delta V$) and V^{liq} and V^{vap} are the liquid and vapour volumes (these volumes depend on the choice of the dividing surface). We will compare values of η^s with values of $(d\gamma/d\tau)$ for a Lennard-Jones system with 256 atoms, in order to see if equation (5.3) is obeyed.

Molecular-dynamics simulations of a liquid–vapour Lennard-Jones system with 256 atoms were performed at different temperatures. A simulation box with sides of length $L_x = 6.7$, $L_y = 6.7$ and $L_z = 13.4$ was used, containing a liquid film with a thickness of about $\Delta z = 6.7$. A shifted potential with a cut-off radius of $R_c = 3$ was employed. First the system was equilibrated by performing 5×10^4 integration time steps (of 10^{-14} s); next, 10^5 integration steps were performed for the determination of the potential energy U, the surface tension γ (using the virial expression (2.8)) and the density profile $\rho(z)$. Each simulation was supplemented by a bulk liquid simulation and a bulk vapour simulation (at the same densities as in the liquid–vapour system) for the determination of the energy densities u^{liq} and u^{vap}. Values of u^{liq} were in agreement with values reported by McDonald and Singer [14] (after correction for the difference in cut-off radius and the shift of the potential).

In table 4, results for the surface tension γ (no long-range correction term is included in these values) and the surface entropy density η^s are presented. In figure 7, γ and η^s are plotted as a function of temperature. The two curves in this figure are fits that are related to each other by the relation $\eta^s = -(d\gamma/d\tau)$ (i.e. equation (5.3)). The slight curvature in the fit of $\gamma(\tau)$ corresponds to a slight decrease with temperature of η^s. This demonstrates that the adsorption equation in the form (5.3) is well obeyed by the small simulation system considered here. It further demonstrates that equation (5.3) provides an accurate method to determine the temperature derivative $(d\gamma/d\tau)$.

5.3. *Binary mixtures*

In this section binary mixtures are considered, with n_a atoms of type 'a' and n_b atoms of type 'b'. We choose the dividing surface so that the adsorption of component b vanishes:

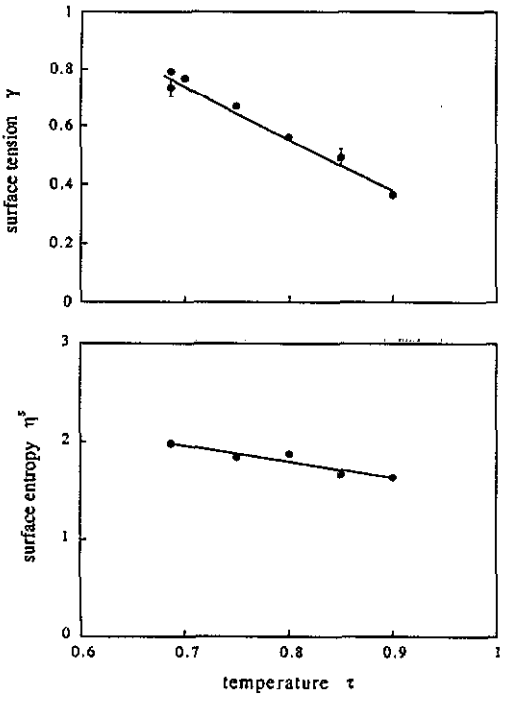

Figure 7. Surface tension γ and surface entropy density η^s of the (truncated and shifted) Lennard-Jones system as a function of temperature τ. The two fits are related by equation (5.3).

$\Gamma_b = 0$. Then the adsorption equation (5.1) reads

$$d\gamma = -\Gamma_a \, d\mu_a \tag{5.6}$$

at constant temperature. The composition of the bulk liquid is represented by the fractional concentrations x_a and x_b, with $x_a + x_b = 1$. For a system with varying composition equation (5.6) can be written as

$$\Gamma_a = -(d\gamma/dx_b)/(d\mu_a/dx_b). \tag{5.7}$$

We will compare values of Γ_a with values of the right-hand side of equation (5.7). The adsorption Γ_a is determined from partial density profiles. Some algebra leads to the following expression (see figure 1):

$$\Gamma_a = \left(\frac{n_a}{A} - \tfrac{1}{2}\rho_a^{vap} L_z\right) - \left(\frac{n_b}{A} - \tfrac{1}{2}\rho_b^{vap} L_z\right) \frac{\rho_a^{liq} - \rho_a^{vap}}{\rho_b^{liq} - \rho_b^{vap}} \tag{5.8}$$

in which ρ_a^{vap} and ρ_b^{vap} are the bulk vapour densities, and ρ_a^{liq} and ρ_b^{liq} are the bulk liquid densities. The differential of the chemical potential in equation (5.7) is determined from the vapour density ρ_a^{vap} through the ideal-gas expression

$$d\mu_a = \tau \, d(\ln \rho_a^{vap}). \tag{5.9}$$

In equilibrium the chemical potential in the liquid is equal to the chemical potential in the vapour.

Simulations were performed on binary systems with 256 atoms, using Lennard-Jones parameters appropriate to the argon–krypton system (a = argon, b = krypton): $\varepsilon_{aa}/\varepsilon_{bb} = 0.763$ (this ratio was also used by Chapela *et al* [2]). For the a–b interaction the Berthelot rule $\varepsilon_{ab} = (\varepsilon_{aa}\varepsilon_{bb})^{1/2}$ was employed. For simplicity, equal atomic sizes were used: $\sigma_{aa} = \sigma_{bb} = \sigma_{ab}$. Five different mixtures were studied: $n_a = 0, 64, 128, 192$ and 256

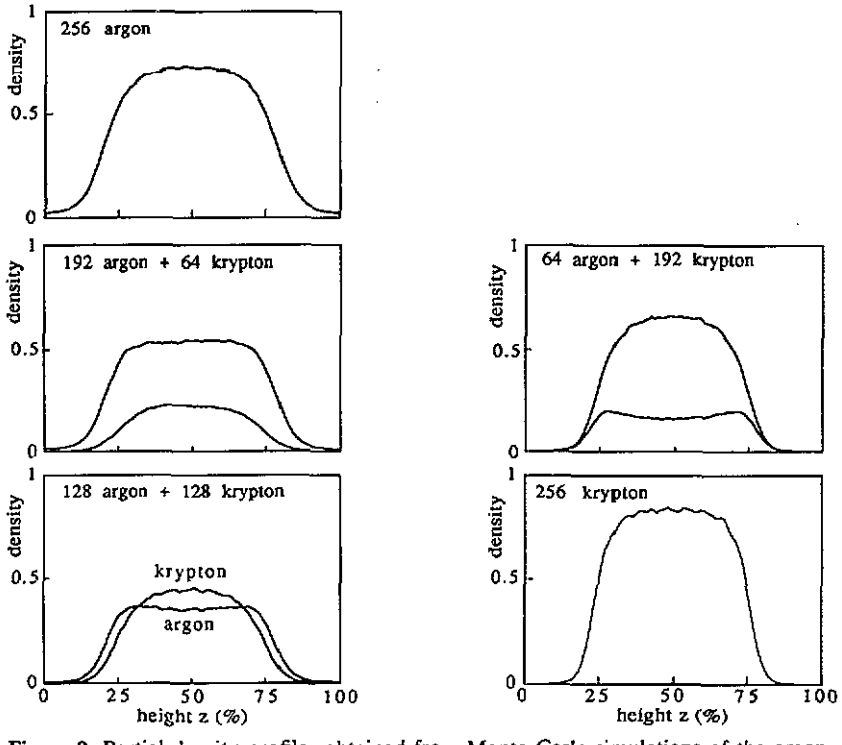

Figure 8. Partial density profiles obtained from Monte Carlo simulations of the argon–krypton system at five different compositions.

Table 5. Surface tension γ and adsorption Γ_a of the argon–krypton system at different compositions, obtained from Monte Carlo simulations described in section 5.3. No long-range correction has been applied. Bulk liquid and vapour partial densities are also indicated.

n_a	γ	ρ_a^{liq}	ρ_b^{liq}	ρ_a^{vap}	ρ_b^{vap}	Γ_a
256	0.418	0.725	0	0.023	0	
192	0.592	0.54	0.22	0.012	0.0010	0.353
128	0.722	0.35	0.44	0.007	0.0022	0.272
64	0.885	0.16	0.66	0.0032	0.0028	0.184
0	1.041	0	0.83	0	0.0020	0

($n_b = 256 - n_a$), at temperature $\tau = 0.9$ ($\tau = kT/\varepsilon_{aa}$; also the quantities γ and μ_a are reduced with respect to ε_{aa}). To enhance interdiffusion in the mixtures, simulations were performed with the variant of the Monte Carlo method described in section 5.1. After each 25 Monte Carlo steps per atom, pairs of dissimilar atoms were considered for an exchange of positions. The simulation box described in section 5.2 was used, and a potential with a cut-off radius of $R_c = 3$. First the system was equilibrated by performing 5×10^4 Monte Carlo steps per atom; next, 2.5×10^5 Monte Carlo steps per atom were performed for the determination of the surface tension (using the virial expression (2.8)) and the partial density profiles.

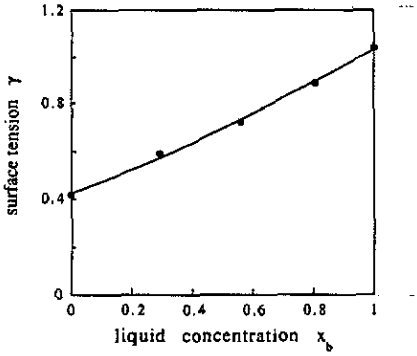

Figure 9. Surface tension γ of the argon–krypton system described in the text as a function of liquid concentration x_b. No long-range correction has been applied.

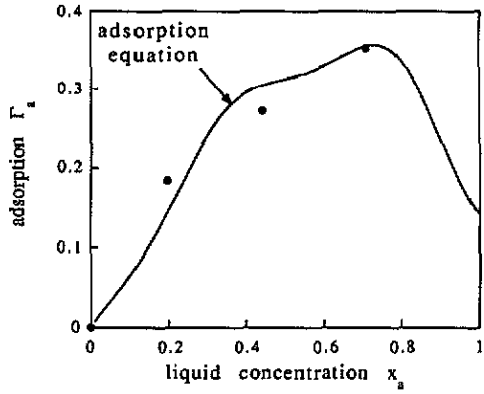

Figure 10. Adsorption Γ_a as a function of liquid concentration x_a: (●) values determined from density profiles; (——) from the adsorption equation.

Figure 8 shows the density profiles obtained for the five different mixtures. In the mixture with 64 argon atoms a significant 'bump' occurs in the argon profile near the liquid–vapour interface. This has also been observed in density profiles calculated from the mean-field theory by Lee *et al* [3]. The bump is consistent with the positive values of the adsorption Γ_a, presented in table 5 together with other results obtained from the similations. In figure 9, the surface tension is plotted as a function of liquid concentration x_b (no long-range correction has been applied). The curve is a fit to the simulation results. Using this fit in equation (5.7), together with a fit to the vapour densities $\rho_a^{vap}(x_b)$, we obtain the curve in figure 10 representing the adsorption Γ_a according to the adsorption equation. The dots in this figure represent the values of Γ_a determined directly from the density profiles, using equation (5.8). The agreement is good, considering the fact that there is a substantial statistical uncertainty (which is difficult to quantify) both in the direct value of Γ_a and in the value given by the adsorption equation.

6. Conclusions

It has been shown that atomistic simulations yield values of interfacial properties of small, phase-segregated systems that are consistent with various thermodynamic relations, within the limits of statistical accuracy.

A new method has been developed for the computation of the liquid–vapour surface tension, which makes use of the Bennett procedure to determine free-energy differences. The method gives a statistical accuracy comparable to the accuracy obtained with the virial expression of the surface tension.

It has been shown that the temperature derivative of the surface tension is determined considerably more accurately by the surface entropy than by the fluctuation equation. Values of the temperature derivative for a system of 256 atoms were found to be in agreement with values predicted by the Gibbs adsorption equation. This agreement is remarkable, considering the small size of the system used to model an inhomogeneous fluid (as mentioned before, consistency with the adsorption equation does not rule out finite-size effects on thermodynamic quantities).

Simulation results for the argon–krypton liquid–vapour system have been presented, which are again consistent with the Gibbs adsorption equation. Partial density profiles for this system were determined by a variant of the Monte Carlo method, in which both displacements and exchanges of atoms are allowed. Positive adsorption of argon manifests itself in krypton-rich mixtures as a significant 'bump' in the density profile near the interface.

We are presently applying the techniques described in this paper to mixtures that do not obey the Berthelot rule and mixtures with differently sized atoms: for these mixtures, excess quantities are expected to be large.

Acknowledgments

We are grateful to G Martin for interesting discussions and for suggesting the use of the Bennett method. We would like to thank V Pontikis for stimulating discussions. Some of the computations were performed at the CIRCE facility, using a grant of FNRS (Belgium) for supercomputers.

References

[1] Rowlinson J S and Widom B 1982 *Molecular Theory of Capillarity* (Oxford: Clarendon)
[2] Chapela G A, Saville G, Thompson S M and Rowlinson J S 1977 *J. Chem. Soc., Faraday Trans. II* **73** 1133
[3] Lee D J, Telo da Gama M M and Gubbins K E 1984 *Mol. Phys.* **53** 1113
[4] Allen M P and Tildesley D J 1987 *Computer Simulation of Liquids* (Oxford: Clarendon)
[5] Kirkwood J G and Buff F P 1949 *J. Chem. Phys.* **17** 338
[6] Schofield P and Henderson J R 1982 *Proc. R. Soc.* A **379** 231
[7] Miyazaki J, Barker J A and Pound G M 1976 *J. Chem. Phys.* **64** 3364
[8] Bennett C H 1976 *J. Comput. Phys.* **22** 245
[9] Fowler R H 1937 *Proc. R. Soc.* A **159** 229
[10] Nijmeijer M J P, Bakker A F, Bruin C and Sikkenk J H 1988 *J. Chem. Phys.* **89** 3789
[11] Liu K S 1974 *J. Chem. Phys.* **60** 4226
[12] Nosé S 1984 *J. Chem. Phys.* **81** 511
[13] Haile J M and Gupta S 1983 *J. Chem. Phys.* **79** 3067
[14] McDonald I R and Singer K 1972 *Mol. Phys.* **23** 29